Reactions of Molybdenum and Tungsten Oxide Tetrafluoride with Sulfur(IV) Lewis Bases: Structure and Bonding in $[WOF_4]_4$, $MOF_4(OSO)$, and $[SF_3][M_2O_2F_9]$ (M = Mo, W)

Douglas Turnbull, [†, ‡] **Praveen Chaudhary,** [†, ‡] **Dakota Leenstra,** [†, ‡] **Paul Hazendonk,** [†, ‡]

Stacey D. Wetmore, [†, ‡] **Michael Gerken*,**[†, ‡]

[†]Canadian Centre for Research in Advanced Fluorine Technologies, University of Lethbridge, 4401 University Drive W, Lethbridge, AB, CA T1K 3M4

[‡]Department of Chemistry and Biochemistry, University of Lethbridge, 4401 University Drive W, Lethbridge, AB, CA T1K 3M4

Canadian Centre for Research in Advanced Fluorine Technologies and the Department of Chemistry and Biochemistry, University of Lethbridge, Lethbridge Alberta, T1K 3M4, Canada.
E-mail: michael.gerken@uleth.ca

ABSTRACT

The structure of $[WOF_4]_4$ has been reinvestigated by low-temperature X-ray crystallography and DFT (MN15/def2-SVPD) studies. Whereas the W_4F_4 ring of the tetramer is planar and disordered in the solid state, the optimised gas-phase geometry prefers a disphenoidally puckered W_4F_4 ring and demonstrates asymmetric fluorine bridging. Dissolution of MOF_4 (M = Mo, W) in SO_2 and SF_4 results in the formation of $MOF_4(OSO)$ and $[SF_3][M_2O_2F_9]$, respectively. Both SO_2 adducts and $[SF_3][Mo_2O_2F_9]$ have been characterised by X-ray crystallography. The crystal structure of $[SF_3][Mo_2O_2F_9]$ reveals dimerisation of the ion pair that results in a rare heptacoordinate sulfur centre. Optimisation of the $\{[SF_3][M_2O_2F_9]\}_2$ dimers in the gas phase, however, results in the elongation of one contact such that the sulfur centres are effectively hexacoordinate. Meanwhile, the crystal structure of $[SF_3][W_2O_2F_9]\cdot HF$ instead demonstrates hexacoordinate sulfur centres and a highly unusual coordination to $[SF_3]^+$ from $[W_2O_2F_9]^-$ through an oxido ligand. While $[SF_3][W_2O_2F_9]$ does not decompose at ambient temperature, $MOF_4(OSO)$ and $[SF_3][Mo_2O_2F_9]$ are unstable towards evolution of SO_2 or SF_4. Computational studies reveal that the monomerisation of $[WOF_4]_4$ in the gas phase at 25 °C is thermodynamically unfavourable using SO_2, but favourable using SF_4, consistent with the relative thermal stabilities of $WOF_4(OSO)$ and $[SF_3][W_2O_2F_9]$.

INTRODUCTION

Sulfur dioxide and tetrafluoride, SO_2 and SF_4, represent quintessential "Lewis-amphoteric" molecules. Both behave as sulfur(IV) Lewis acids towards nitrogen bases, allowing for the isolation and characterisation of numerous adducts,[1–4] but also as O/F-donors towards strong Lewis acids such as AsF_5 and SbF_5.[5,6] In the case of SF_4, its Lewis basicity under such circumstances manifests as discrete F^- donation to form $[SF_3]^+$ salts,[5] whereas SO_2 instead forms molecular adducts, as exemplified in the crystal structure of $SbF_5(OSO)$.[7] The versatile O-donor/S-acceptor behaviour of SO_2 is perhaps best demonstrated by its reaction with frustrated Lewis pairs to afford zwitterionic sulfinate esters.[8] Sulfur dioxide also behaves as an ambidentate (κ^1-S, κ^1-O, and η^2-S,O) or bridging O,O ligand towards various *s*-, *d*- and *f*-block metals,[9–12] whereas SF_4 oxidatively adds across Rh^I, Ir^I, and Pt^0 complexes to afford the $S^{II}F_3$ ligand.[13]

Lewis acid-base adducts of SO_2 have found synthetic utility: the $(SO_2)_2{\cdot}$DABCO (DABCO = diazabicyclo[2.2.2]octane) adduct behaves as a solid synthetic equivalent to SO_2, a toxic gas under ambient conditions, in the preparation of sulfonamides ($RSO_2(NR'_2)$) and sulfamides ($SO_2(NR_2)_2$).[14] Conversely, SO_2 monomerises the viscous liquid $[SbF_5]_4$ to afford solid $SbF_5(OSO)$,[6] which has been used to conveniently abstract F^- from $WF_6(L)$ (L = 2,2′-bipyridine; 1,10-phenanthroline) in the preparation of $[WF_5(L)]^+$ salts.[15] The crystal structure of $(SO_2)_2{\cdot}$DABCO[14] reveals two S···N chalcogen bonds per DABCO molecule, resulting in symmetric weakening of the S=O bonds (1.450(1)–1.455(2) Å) with respect to SO_2 (1.4299(3) Å).[16] In contrast, κ^1-O coordination to SbF_5 results in substantial polarisation of the SO_2 molecule, weakening the coordinated S=O bond (1.469(4) Å) and complementarily strengthening the terminal S=O bond (1.402(4) Å).[7]

Like SbF_5, WOF_4 is known to aggregate by way of fluorine bridges under standard conditions, yielding $[WOF_4]_4$.[17] The original crystal structure, in which C_{2h} symmetry is crystallographically imposed on the tetramer, was incorrectly interpreted on the basis of oxygen bridging between tungsten centres.[17] However, vibrational-spectroscopic studies elucidated the presence of terminal oxido and bridging fluorido ligands soon thereafter.[18,19] Recently, there has been a resurgence in exploration of the coordination chemistry of high-valent group-6 fluorides and oxide fluorides, i.e. MO_nF_{6-2n} (M = Cr, Mo, W; n = 0–2), demonstrating the capabilities of MOF_4 as Lewis acids under formation of hexa- and/or heptacoordinate adducts.[20–23] Notably, the first crystallographically characterised examples of $[CrOF_5]^-$,[24] $[Mo_2O_2F_9]^-$,[24,25] and ordered $[WOF_5]^-$[24,26] salts were reported, as well as superior-quality structures of $[W_2O_2F_9]^-$ salts.[24,27]

Though a preliminary account exists for the formation of $[SF_3][W_2O_2F_9]$ upon reaction of WOF_4 with SF_4, the ionic formulation of which was confirmed by ^{19}F NMR spectroscopy,[28] the structural characteristics of the salt have yet to be elucidated. Herein, we report the synthesis and characterisation of $MOF_4(OSO)$ and $[SF_3][M_2O_2F_9]$ as well as a crystallographic reinvestigation of $[WOF_4]_4$. To our knowledge, these represent the first conclusively characterised examples of SO_2 adducts and $[SF_3]^+$ salts of d^0 transition-metal complexes. Density-functional-theory (B3LYP) studies have been undertaken to elucidate the structure of $[WOF_4]_4$, investigate its monomerisation by SO_2 and SF_4, and elucidate the bonding characteristics of $[WOF_4]_4$, $MOF_4(OSO)$, and $[SF_3][M_2O_2F_9]$.

RESULTS AND DISCUSSION

Synthesis and Properties of $MOF_4(OSO)$ and $[SF_3][M_2O_2F_9]$ (M = Mo, W). The $WOF_4(OSO)$ adduct was synthesised during an attempt to recrystallise $[WOF_4]_4$ from SO_2 at –30 °C, followed by removal of the solvent at or below that temperature under dynamic vacuum (Eq. 1). It manifests

as a white solid that is highly soluble in SO_2 which, unlike other WOF_4 adducts with N-, P-, and O-donor ligands, is susceptible to loss of SO_2 above *ca.* –20 °C under *ca.* 700 Torr N_2, as determined by Raman spectroscopy. Prolonged exposure to dynamic vacuum at ambient temperature results in complete reversion to the starting materials. The $MoOF_4(OSO)$ adduct could be prepared analogously from $MoOF_4$ and SO_2; its physical properties are largely similar.

$$MOF_4 + SO_2 \rightleftharpoons MOF_4(OSO)\ (M = Mo, W) \quad (1)$$

The $[SF_3][M_2O_2F_9]$ salts were prepared upon dissolution of MOF_4 in SF_4 at –30 °C (Eq. 2) and could be isolated upon removal of excess SF_4 at –80 °C as white solids that are soluble in SO_2, SF_4, and anhydrous HF (aHF). Crystallisation of $[SF_3][W_2O_2F_9]$ from aHF and aHF/SF_4 yields the $[SF_3][W_2O_2F_9]\cdot HF$ solvate, whereas $[SF_3][Mo_2O_2F_9]$ is not solvated after crystallisation from aHF/SF_4. While $[SF_3][W_2O_2F_9]$ does not decompose at ambient temperature, $[SF_3][Mo_2O_2F_9]$ loses SF_4 over the course of hours, returning $MoOF_4$. There is no evidence for the oxidation of SO_2 or SF_4 by MOF_4 under ambient conditions.

$$2MOF_4 + SF_4 \rightarrow [SF_3][M_2O_2F_9]\ (M= Mo, W) \quad (2)$$

Despite the reactions occurring in the presence of a large excess of SF_4, $[SF_3][M_2O_2F_9]$ are formed quantitatively, with no evidence of $[SF_3][MOF_5]$. In contrast, reactions of MOF_4 with the fluoride-ion source NOF in aHF yielded mixtures of $[M_2O_2F_9]^-$, $[MOF_5]^-$, and $[MOF_6]^{2-}$. The relative amounts of each anionic species depended on the $[F(HF)_n]^-$ concentration.[29] In the most fluoroacidic conditions, $[M_2O_2F_9]^-$ were favoured due to F^- abstraction from $[MOF_5]^-$ and $[MOF_6]^{2-}$, suggesting that $[SF_3]^+$ is sufficiently fluoroacidic to destabilise $[SF_3][MOF_5]$ and $[SF_3]_2[MOF_6]$ towards loss of SF_4.

Crystal and Molecular Structures. The structures of $[WOF_4]_4$, $MOF_4(OSO)$ (M = Mo, W), $[SF_3][Mo_2O_2F_9]$, and $[SF_3][W_2O_2F_9]\cdot HF$ were investigated by X-ray crystallography at –173 °C.

Crystallographic data collection and refinement parameters are provided in Table S1. In addition, the geometries of monomeric MOF_4, $[WOF_4]_4$, $MOF_4(OSO)$, and $[SF_3][M_2O_2F_9]$ were optimised at the MN15/def2-SVPD level of theory, resulting in excellent agreement between the experimental and calculated data. Experimental and calculated geometric parameters are given for $[WOF_4]_4$, $MOF_4(OSO)$, $[SF_3][M_2O_2F_9]$, and $[SF_3][W_2O_2F_9]\cdot HF$ are given in Tables 1–4, respectively.

The gas-phase geometries of monomeric MOF_4 are predicted to be square-pyramidal with an apical oxido ligand (Mo=O: 1.637, Mo–F: 1.834 Å, O–Mo–F: 104.6°; W=O: 1.670, W–F: 1.855 Å, O–W–F: 104.4°). This is highly comparable to the gas-phase electron-diffraction data reported previously for MOF_4 (e.g. WOF_4; W=O: 1.666(7), W–F: 1.847(2) Å, O–W–F: 104.8(6)°)[30] as well as a recent computational study at the PBE0/def2-SVP level of theory.[24]

The low-temperature crystal structure of $[WOF_4]_4$ reveals no transition from the disordered *C*2/*m* ambient-temperature phase reported by Edwards and Jones.[17] As such, it is invariably isotypic with $[MF_5]_4$ (M = Nb, Mo, Ta, W;[31] Figure 1a). The W–F_b (b = bridging) bond lengths (2.111(3), 2.122(3) Å) would suggest symmetric fluorine bridging between tungsten centres, which is observed crystallographically for $[MF_5]_4$ and recently predicted in the gas phase for $[MoF_5]_4$[32] and $[WF_5]_4$.[33] Symmetric bridging is, however, in contrast to the expected *trans* influence of the W=O bond in the W−F_b···W=O moiety.

Optimisation of C_{4h}-symmetric $[WOF_4]_4$ in the gas phase reveals highly asymmetric bridging (1.963, 2.265 Å) for which the average bond length (2.115 Å) agrees well with the crystallographic data (Figure 1b). The calculated W=O (1.669 Å) and terminal W–F_t (t = trans-to-bridging, 1.837 Å) bonds have an average length (1.753 Å) that is comparable to the disordered W–O(1)/F(1) bond lengths observed in the crystal structure (1.737(3), 1.746(3) Å). The O/F_t and

W–F_b···W disorders are reflected in the elongated thermal ellipsoids of the tungsten atoms, rather than those of the F_b and disordered O/F_t atoms. This is a consequence of displacement of tungsten from the octahedral centres to contract the W=O and W–F_b bonds and elongate the W–F_t and W···F_b bonds. Attempts to model this disorder using split positions for tungsten were unsuccessful. The ordered W–F_c bond lengths (c = cis-to-bridging; exptl. 1.822(4)–1.840(4), calcd. 1.849 Å) agree well with the predicted values. Comparison of the optimised structures of mono- and tetrameric WOF_4 reveals negligible change in the W=O and W–F_c bonds. However, the bridging interactions result in an elongation of the intramolecular W–F_b bond and complementary contraction of the opposing W–F_t bond.

Whereas the W_4F_4 ring in $[WOF_4]_4$ is planar in the solid state, optimisation of a C_{4h}-symmetric tetramer reveals six imaginary vibrational modes that correspond to a disphenoidal ring puckering and descent from C_{4h} to C_2 symmetry. Optimisation of a puckered tetramer returns a ground-state geometry that is 18 kJ mol^{-1} lower in energy. Despite the considerable puckering, which substantially reduces the W–F–W angle from 169.5 to 142.3°, the effects on the local geometries of the tungsten centres are negligible.

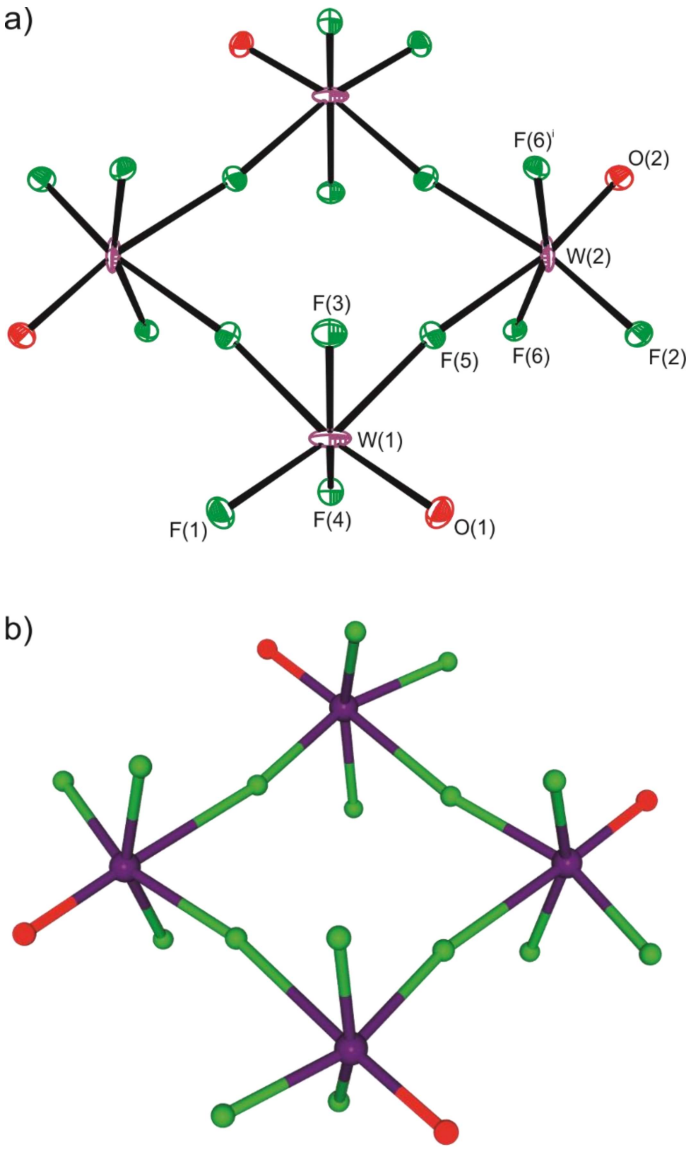

Figure 1. Structure of $[WOF_4]_4$: a) thermal ellipsoid plot (50% probability level) and b) optimised gas-phase geometry (MN15/def2-SVPD, C_{4h} symmetry).

Table 1. Selected Bond Lengths (Å) and Angles (°) of $[WOF_4]_4$[a]

	exptl	calcd (C_{4h})[b,c]	calcd (C_2)[b]		exptl	calcd (C_{4h})[b,c]	calcd (C_2)[b]
W(1)–O(1)[d]	1.738(3)	1.669	1.669	O(1)–W(1)–F(1)	101.4(2)	100.5	100.9
W(2)–O(2)[d]	1.746(3)	1.669	1.669	O(1)–W(1)–F(3)	96.94(15)	100.9	101.0
W(1)–F(1)[d]	1.738(3)	1.837	1.835	O(1)–W(1)–F(4)	95.48(14)	100.9	100.8
W(2)–F(2)[d]	1.746(3)	1.837	1.835	O(1)–W(1)–F(5)	89.36(14)	98.0	97.9
W(1)–F(3)	1.822(4)	1.849	1.848	F(1)–W(1)–F(5)	169.17(14)	161.5	161.2
W(1)–F(4)	1.842(4)	1.849	1.851	F(3)–W(1)–F(4)	160.32(19)	156.6	156.4
W(1)–F(5)	2.110(3)	1.963	1.970	F(3)–W(1)–F(5)	82.31(13)	84.4	84.0
W(2)–F(5)	2.123(3)	2.266	2.264	F(5)–W(1)–F(5)[j]	79.82(16)	79.5	78.0
W(2)–F(6)	1.835(3)	1.849	1.851	W(1)–F(5)–W(2)	170.14(16)	169.5	142.3

[a]Symmetry transformation: j = x, 1 – y, z. [b]Calculated at the MN15/def2-SVPD level of theory. [c]Sixth-order saddle point. [d]O(1) and O(2) exhibit unresolved disorder with F(1) and F(2), respectively.

The $MOF_4(OSO)$ adducts are crystallographically isotypic and crystallise in the monoclinic space group $P2_1/c$ with four molecules per unit cell. Despite β closely approximating 90° in both cases, there is no evidence for twinning by pseudomerohedry. Consistent with the ^{19}F NMR spectroscopic data (*vide infra*), $MOF_4(OSO)$ adopt octahedral structures in which the SO_2 ligand is positioned *trans* to the oxido ligand, a coordination motif that is ubiquitous for hexacoordinate MOF_4 adducts (Figure 2). The SO_2 ligand is effectively staggered with respect to the MF_4 moiety (θ[F(1)–M–O(2)–S]; M = Mo: 65.08(12), W: 61.5(3)°).

The W=O bond (1.660(4) Å) in $WOF_4(OSO)$ is shorter than in $WOF_4\{OP(C_6H_5)_3\}$ (1.682(5) Å),[20] $WOF_4(NC_5H_5)$ (1.690(3) Å),[34] and ordered $[WOF_5]^-$ in [1,10-phen][WOF_5] (1.698(2) Å)[26] and $[Xe_2F_{11}][WOF_5]$ (1.698(3) Å).[24] Similarly, the Mo=O bond of $MoOF_4(OSO)$ (1.6465(14) Å) is slightly shorter than those of $MoOF_4\{OP(C_6H_5)_3\}$ (1.6643(18) Å)[35] and $[Xe_2F_{11}][MoOF_5]$ (1.664(3) Å).[24] In contrast, the M···O contact distances of $MOF_4(OSO)$ (M = Mo: 2.3988(12), W: 2.381(3) Å) are substantially longer than in the $(C_6H_5)_3PO$ adducts (M = Mo: 2.1533(16),[35] W: 2.141(4) Å[20]). This indicates that the M···O contacts in the SO_2 adducts are weak and SO_2 has a minimal *trans* influence on the M=O bonds. The M–F bonds of $MoOF_4(OSO)$

(1.8403(10)–1.8631(11) Å) and $WOF_4(OSO)$ (1.844(3)–1.867(3) Å) are indistinguishable from previously reported complexes (*ca*. 1.84–1.87 Å). The SO_2 molecule (S=O in free SO_2: 1.4299(3) Å)[16] is polarised in $MOF_4(OSO)$ (M = Mo: 1.4483(13), 1.4160(14); W: 1.448(3), 1.417(4) Å), though to a lesser extent than in $SbF_5(OSO)$ (1.469(4), 1.402(4) Å).[7]

Optimisation of $MOF_4(OSO)$ in the gas phase returns C_s-symmetric, octahedral structures that are in excellent agreement with the crystallographic data, the largest discrepancies being minor overestimations of the M···O contact distances (within 0.06 Å). The SO_2 ligands are perfectly staggered with respect to the MF_4 moiety (θ[F(1)–M–O(2)–S] = 45°) and their weak basicities are evidenced by the similarity of the optimised M=O (M = Mo: 1.640, W: 1.674 Å) and M–F (M = Mo: 1.839, 1.846; W: 1.860, 1.867 Å) bond lengths in $MOF_4(OSO)$ to those of free MOF_4 in the gas phase (*vide supra*).

Table 2. Selected Bond Lengths (Å) and Angles (°) of $MOF_4(OSO)$ (M = Mo, W)

	M = Mo		M = W			M = Mo		M = W	
	exptl	**calcd[a]**	**exptl**	**calcd[a]**		**exptl**	**calcd[a]**	**exptl**	**calcd[a]**
M–O(1)	1.6465(14)	1.640	1.671(4)	1.674	O(1)–M–F(1)	101.22(6)	101.9	101.41(15)	101.7
M–F(1)	1.8429(11)	1.846	1.844(3)	1.867	O(1)–M–F(2)	100.72(5)	102.0	100.72(14)	101.9
M–F(2)	1.8520(11)	1.839	1.865(3)	1.860	O(1)–M–F(3)	100.25(6)	102.0	100.43(15)	101.9
M–F(3)	1.8631(11)	1.839	1.867(3)	1.860	O(1)–M–F(4)	100.91(6)	101.9	100.74(18)	101.7
M–F(4)	1.8403(10)	1.846	1.854(3)	1.867	O(1)–M–O(2)	179.02(6)	179.5	178.90(15)	179.3
M–O(2)	2.3988(12)	2.454	2.381(3)	2.439	F(1)–M–F(2)	88.68(5)	87.5	88.58(13)	87.6
S–O(2)	1.4483(13)	1.466	1.448(3)	1.468	F(1)–M–F(3)	158.51(5)	156.1	158.15(14)	156.5
S–O(3)	1.4160(14)	1.443	1.417(4)	1.442	F(1)–M–F(4)	89.29(5)	87.4	89.41(12)	87.4
					F(1)–M–O(2)	79.47(4)	77.8	79.28(12)	77.8
					M–O(2)–S	140.20(7)	132.7	141.00(19)	133.1
					O(2)–S–O(3)	117.44(8)	117.3	117.1(2)	117.2

[a]Calculated at the MN15/def2-SVPD level of theory.

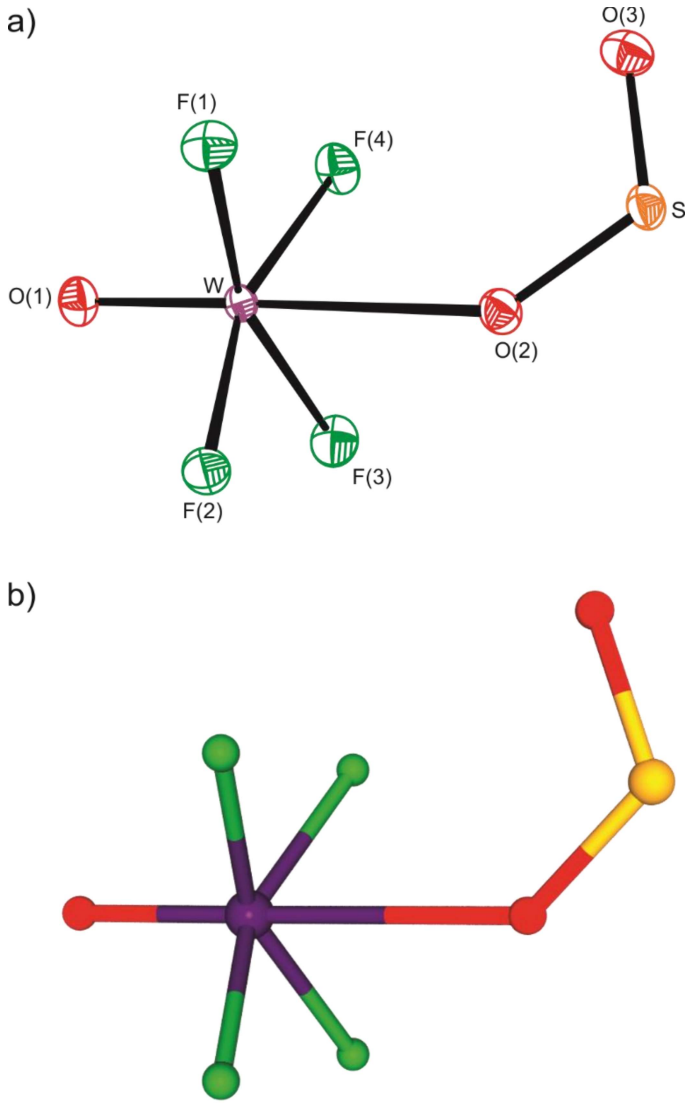

Figure 2. Structure of $WOF_4(OSO)$: a) thermal ellipsoid plot (50% probability level) and b) optimised gas-phase geometry (MN15/def2-SVPD). Note that $MoOF_4(OSO)$ is isostructural.

The $[SF_3][Mo_2O_2F_9]$ salt crystallises from aHF/SF_4 in the monoclinic space group $P2_1/n$ with four ion pairs per unit cell. The asymmetric unit consists of an ion pair that is associated via S···F chalcogen-bonding interactions such that $[SF_3]^+$ is chelated by $[Mo_2O_2F_9]^-$ (κ^2-F). Each ion forms two further contacts to two neighbouring counterions (Figure 3a), resulting in a dimeric structural unit like that in $[XeF_5][M_2O_2F_9]$.[24] Interestingly, this results in a rare heptacoordinate sulfur(IV) centre, rather than the hexacoordinate moieties observed in $[SF_3][BF_4]$,[36]

$[SF_3]_2[GeF_6]$,[37] and $[SF_3(NSF_3)_2][AsF_6]$,[38] as well as SF_4 adducts with O-donors[39] and hexamethylenetetramine.[4] The S···F contacts, either within (2.4723(10), 2.4937(10) Å) or between (2.8453(9), 2.9292(10) Å) ion pairs, are significantly shorter than the sum of the van der Waal's radii (3.35 Å).[40]

The $[Mo_2O_2F_9]^-$ anion adopts a bent, dioctahedral geometry with the oxido and bridging fluorido ligands in axial positions, as observed previously.[24,25] The equatorial MoF_4 moieties are eclipsed with respect to one another, as in the $[XeF_5]^+$ salt, but unlike the alkali-metal salts. The Mo–F_{ax}–Mo bridge is only slightly asymmetric (2.1392(9), 2.1466(9) Å). The equatorial Mo–F bonds can be differentiated in terms of short, terminal (1.8325(10)–1.8501(9) Å); medium-length, weak Mo–F···S bridging (1.8570(9)–1.8584(9) Å); and long, "strong" Mo–F···S bridging (1.8989(9)–1.8990(9) Å) environments due to their various degrees of interaction with $[SF_3]^+$. The Mo–F_{ax} bonds are significantly longer than their equatorial counterparts due to the *trans* influences of the oxido ligands as well as three-centre, four-electron bonding between the two molybdenum centres. Despite the lack of approximate C_{3v} symmetry about the sulfur centre due to the unusual fluorine-bridging motif, the geometry of the cation is still a regular trigonal pyramid with insignificantly different S–F bond lengths (1.5102(9)–1.5144(9) Å) and similar F–S–F angles (96.57(5)–97.65(5)°). The S–F, Mo=O, and Mo–F bond lengths are within the ranges observed for previously reported crystal structures of $[SF_3]^+$ and $[Mo_2O_2F_9]^-$ salts, as are the internal angles, including the Mo–F_{ax}–Mo angle (153.09(5)°).

Optimisation of the $\{[SF_3][Mo_2O_2F_9]\}_2$ dimer in the gas phase results in a pseudo-C_i-symmetric geometry that agrees well with the crystal structure of $[SF_3][Mo_2O_2F_9]$, excellently reproducing the S–F, Mo=O, and Mo–F bonds (Table 3). The largest geometric disparities are a twist of the $[Mo_2O_2F_9]^-$ anions to accommodate a staggering of the MF_4 moieties as well as a slight

change of the coordination about the sulfur centre. The two S···F contacts within each ion pair are accurately predicted (2.474, 2.497 Å), whereas one contact between the pairs is underestimated (2.550, 2.956 Å), resulting in a more typical hexacoordinate motif about the sulfur centres along with an additional weak contact. The $\{[SF_3][W_2O_2F_9]\}_2$ dimer is predicted to be isostructural in the gas phase with comparable S–F bonds and S···F contacts. The W=O and W–F bonds agree with calculated data for $\{[XeF_5][W_2O_2F_9]\}_2$.[24]

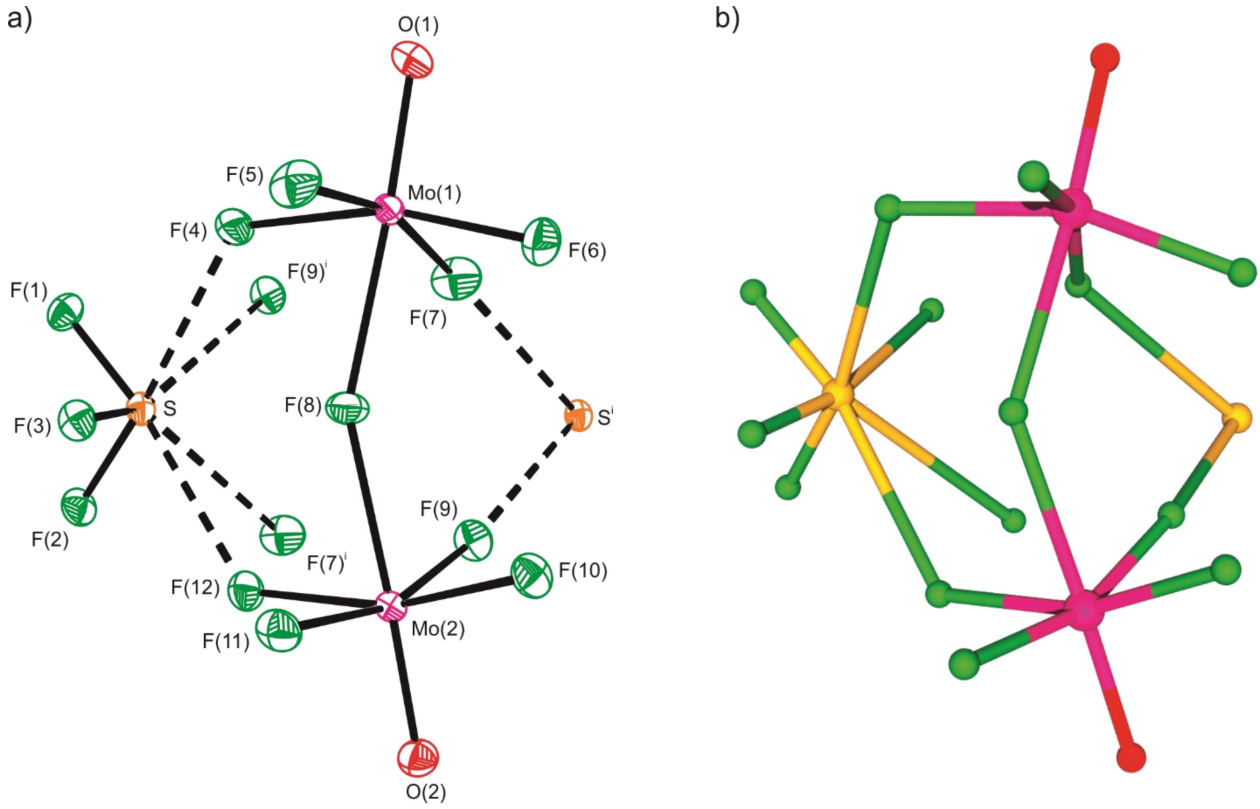

Figure 3. Structure of $[SF_3][Mo_2O_2F_9]$: a) thermal ellipsoid plot (50% probability level) and b) optimised gas-phase geometry (MN15/def2-SVPD) of one half of the $\{[SF_3][Mo_2O_2F_9]\}_2$ dimer. The second half is omitted for clarity, except for $F(7)^i$, $F(9)^i$, and S^i, in both a) and b). Secondary bonding interactions are indicated by dashed lines (---) in a). Note that $\{[SF_3][W_2O_2F_9]\}_2$ is predicted to be isostructural.

Table 3. Selected Bond Lengths (Å) and Angles (°) of $[SF_3][M_2O_2F_9]$ (M = Mo, W)[a]

	M = Mo		M = W		M = Mo		M = W
	exptl	calcd[b]	calcd[b]		exptl	calcd[b]	calcd[b]
S–F(1)	1.5144(9)	1.549	1.547	F(1)–S–F(2)	96.57(5)	94.6	95.1
S–F(2)	1.5121(9)	1.546	1.544	F(1)–S–F(3)	97.36(5)	95.1	95.2
S–F(3)	1.5102(9)	1.544	1.544	F(2)–S–F(3)	97.65(5)	96.4	96.5
M(1)–O(1)	1.6522(11)	1.645	1.677	O(1)–M(1)–F(4)	96.57(5)	98.5	98.8
M(2)–O(2)	1.6532(11)	1.645	1.677	O(1)–M(1)–F(5)	98.94(5)	99.4	99.6
M(1)–F(4)	1.8990(9)	1.905	1.918	O(1)–M(1)–F(6)	99.87(5)	100.4	100.2
M(1)–F(5)	1.8413(9)	1.826	1.847	O(1)–M(1)–F(7)	97.81(5)	98.3	98.5
M(1)–F(6)	1.8325(10)	1.830	1.851	O(1)–M(1)–F(8)	175.91(5)	175.6	175.9
M(1)–F(7)	1.8570(9)	1.874	1.894	F(4)–M(1)–F(5)	87.81(4)	89.1	89.4
M(1)–F(8)	2.1466(9)	2.142	2.154	F(4)–M(1)–F(6)	163.54(4)	160.1	160.0
M(2)–F(8)	2.1392(9)	2.127	2.140	F(4)–M(1)–F(7)	86.86(4)	82.8	82.9
M(2)–F(9)	1.8584(9)	1.893	1.912	F(4)–M(1)–F(8)	79.48(4)	77.4	77.5
M(2)–F(10)	1.8373(9)	1.825	1.846	M(1)–F(8)–M(2)	153.09(5)	141.0	141.9
M(2)–F(11)	1.8501(9)	1.827	1.848				
M(2)–F(12)	1.8989(9)	1.897	1.913				
S···F(4)	2.4723(10)	2.474	2.494				
S···F(7)^{i}	2.9292(10)	2.956	2.960				
S···F(9)^{i}	2.8453(9)	2.550	2.538				
S···F(12)	2.4937(10)	2.497	2.512				

[a]Symmetry transformation: i = 1 – x, 1 – y, 1 – z. [b]Calculated at the MN15/def2-SVPD level of theory.

Table 4. Selected Bond Lengths (Å) and Angles (°) of $[SF_3][W_2O_2F_9]\cdot HF$[a]

	exptl		exptl
S–F(1)	1.509(3)	F(1)–S–F(2)	97.38(14)
S–F(2)	1.527(3)	F(1)–S–F(3)	96.94(16)
S–F(3)	1.509(3)	F(2)–S–F(3)	97.02(15)
W(1)–O(1)	1.694(3)	O(1)–W(1)–F(5)	96.96(13)
W(2)–O(2)	1.684(3)	O(1)–W(1)–F(6)	97.81(14)
W(1)–F(5)	1.884(3)	O(1)–W(1)–F(7)	98.63(13)
W(1)–F(6)	1.847(3)	O(1)–W(1)–F(8)	97.42(14)
W(1)–F(7)	1.846(2)	O(1)–W(1)–F(9)	177.87(12)
W(1)–F(8)	1.854(3)	F(5)–W(1)–F(6)	88.40(12)
W(1)–F(9)	2.095(2)	F(5)–W(1)–F(7)	164.40(12)
W(2)–F(9)	2.146(2)	F(5)–W(1)–F(8)	87.73(12)
W(2)–F(10)	1.838(3)	F(5)–W(1)–F(9)	80.97(11)
W(2)–F(11)	1.886(3)	W(1)–F(9)–W(2)	172.46(15)
W(2)–F(12)	1.861(3)		
W(2)–F(13)	1.847(3)		
S···F(4)^{i}	2.489(3)	F(1)–S···F(4)^{i}	176.72(13)
F(4)···F(5)	2.568(4)	F(4)–H(4)···F(5)	167(6)
H(4)···F(5)	1.78(6)	S···O(1)^{j}–W(1)^{j}	175.30(19)
S···O(1)^{j}	2.536(3)	S···F(11)–W(2)	169.82(14)
S···F(11)	2.474(3)		

[a]Symmetry transformations: i = 2.5 – x, y – 0.5, 1.5 – z; j = 0.5 + x, y, z.

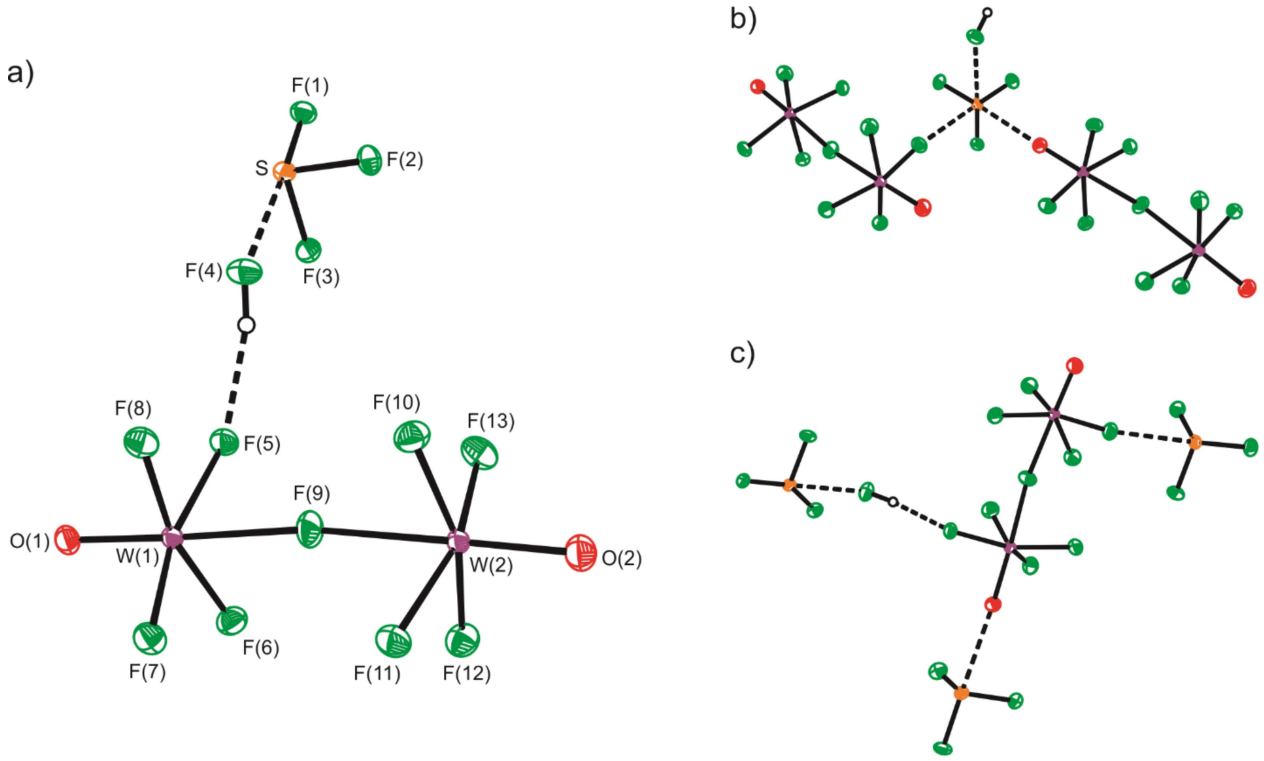

Figure 4. Thermal ellipsoid plot (50% probability level) of a) one of two $[SF_3][W_2O_2F_9]\cdot HF$ ion pairs in the asymmetric unit with secondary bonding interactions (dashed lines, ---) to b) $[SF_3]^+$ and c) $[W_2O_2F_9]^-$.

Whereas attempts to crystallise $[SF_3][W_2O_2F_9]$ from SF_4 were unsuccessful, crystallisation from aHF or aHF/SF_4 resulted in insertion of HF into a cation-anion contact and the formation of $[SF_3][W_2O_2F_9]\cdot HF$ (Figure 4a). The solvate crystallises in the monoclinic space group $P2_1/n$ with two ion pairs and solvent molecules per asymmetric unit. Each ion pair associates with neighbouring pairs and HF such that sulfur forms three chalcogen bonds: two from $[W_2O_2F_9]^-$ (κ^1-O and κ^1-F) and a third from HF (Figure 4b). Correspondingly, each anion is coordinated to one molecule of HF and two cations (Figure 4c), similar to $[SF_3][SbF_6]\cdot HF$.[41] In particular, the S···O chalcogen-bonding interactions are noteworthy, as hitherto $[M_2O_2F_9]^-$ have only been reported to coordinate via the equatorial fluorido ligands. The chelation observed in $[SF_3][Mo_2O_2F_9]$ does not occur in $[SF_3][W_2O_2F_9]\cdot HF$.

Like $[SF_3][Mo_2O_2F_9]$, the S–F, W=O, and W–F bond lengths are within the ranges of previously reported $[SF_3]^+$ and $[W_2O_2F_9]^-$ salts,[24,27,42–44] and the W–F bonds involved in hydrogen- or chalcogen-bonding interactions (1.884(3)–1.889(3) Å) are longer than the unaffected W–F bonds (1.837(3)–1.864(3) Å). Chalcogen bonding results in a slight elongation of one W=O bond (1.684(3)–1.694(3) Å). The tungsten centres are asymmetrically fluorine bridged (2.146(2), 2.095(2) and 2.150(2), 2.098(2) Å). This could be induced by coordination of one oxido ligand, though asymmetries of similar magnitude were observed in the $[XeF_5]^+$ salts, for which analogous Xe···O interactions were not observed.[24] The $[W_2O_2F_9]^-$ anions in $[SF_3][W_2O_2F_9]\cdot HF$ are nearly linear (W–F–W: 169.91(15), 172.46(15)°), as opposed to the bent geometries observed in unsolvated $[SF_3][Mo_2O_2F_9]$ and predicted for $\{[SF_3][W_2O_2F_9]\}_2$ (*vide supra*).

Raman Spectroscopy. The Raman spectrum of solid $[WOF_4]_4$ (Figure S1) was reacquired at ambient temperature and those of $MOF_4(OSO)$ (Figure 5), $[SF_3][M_2O_2F_9]$ (Figure 6), and $[SF_3][W_2O_2F_9]\cdot HF$ (Figure S3) were acquired at −100 °C. In addition, vibrational frequencies were calculated for $[WOF_4]_4$, $MOF_4(OSO)$, and $\{[SF_3][M_2O_2F_9]\}_2$ at the MN15/def2-SVPD level of theory, generally resulting in only minor overestimations of the stretching modes and accurate approximations of the bending/deformation modes, allowing for their unambiguous assignment. Vibrational frequencies, with assignments, are provided in the Supporting Information (Tables S2–S4).

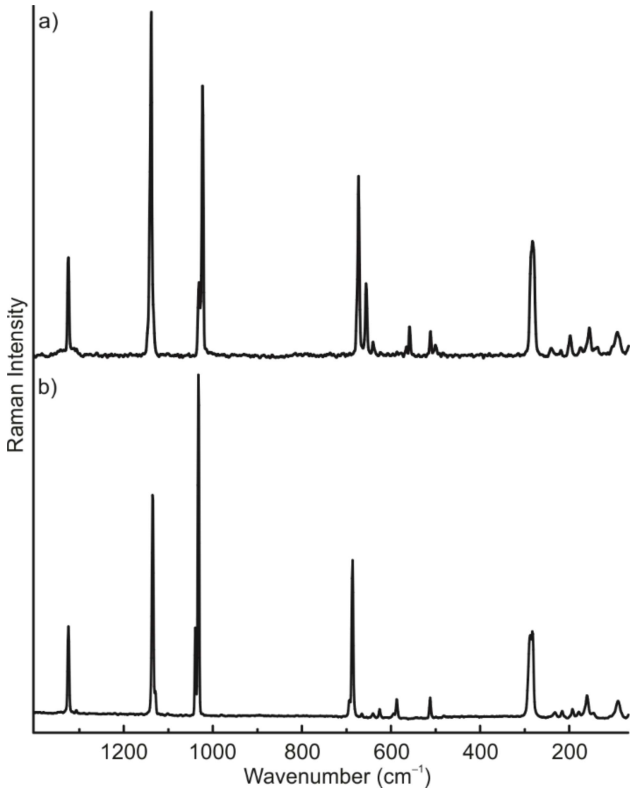

Figure 5. Raman spectra of solid $MOF_4(OSO)$, recorded at –100 °C: a) M = Mo, b) M = W.

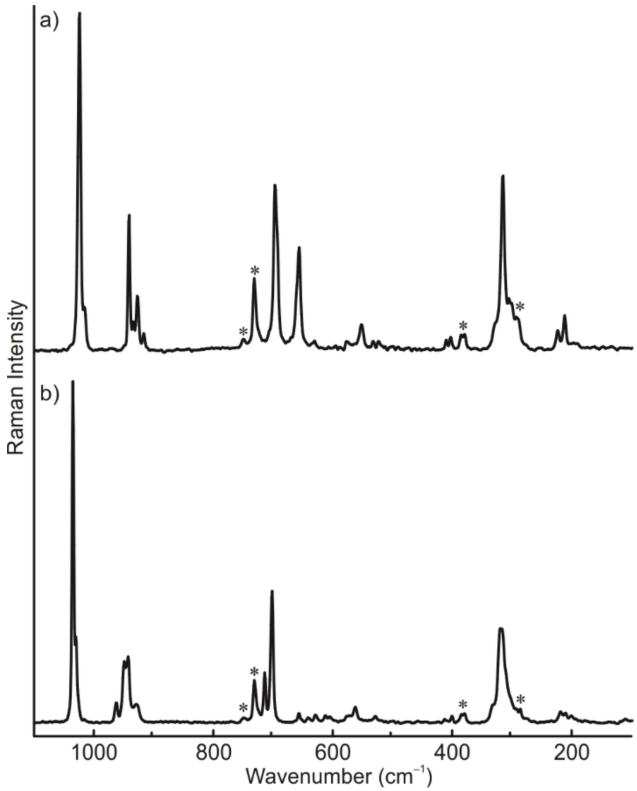

Figure 6. Raman spectra of solid $[SF_3][M_2O_2F_9]$, recorded at −100 °C: a) M = Mo, b) M = W. Asterisks (*) denote FEP sample tube bands.

The Raman spectrum of $[WOF_4]_4$ is in excellent agreement with previously reported data[45] and its vibrations have been unambiguously assigned on the basis of a tetrameric structure (Table S2). Of the four possible W=O stretching modes, two are predicted to possess substantial Raman intensity, which are separated by only 4 cm^{-1}, consistent with the observation of a single Raman band in the experimental spectrum.

Adduct formation of MOF_4 with SO_2 results in minimal changes to the vibrational frequencies of the M=O (M = Mo: 1040, 1032; W: 1048, 1041 cm^{-1}) and symmetric M–F (M = Mo: 691, 674; W: 711, 704 cm^{-1}) stretching modes with respect to those of the parent MOF_4 in the solid state (M = Mo: 1039, 706–716;[45] W: 1056, 704–741 cm^{-1}). Complementarily, the S=O

stretching frequencies of solid SO_2 (1324, 1148 cm^{-1})[46] are effectively unperturbed by coordination to MOF_4 (M = Mo: 1326, 1144; W: 1326, 1309, 1142, 1137 cm^{-1}). The S=O stretching modes of $WOF_4(OSO)$ are split due to $^{32/34}S$ isotope effects, which were replicated excellently in frequency calculations for $WOF_4(O^{32}SO)$ and $WOF_4(O^{34}SO)$ ($\Delta\bar{\nu}[\nu_{as}(SO_2)]$: exptl: 17; calcd. 15 cm^{-1}; $\Delta\bar{\nu}[\nu_s(SO_2)]$: exptl: 5; calcd. 8 cm^{-1}). No such splittings were observed for $MoOF_4(OSO)$.

The symmetric S–F (M = Mo: 918–943, W: 931–964 cm^{-1}), M=O (M = Mo: 1026, 1020; W: 1036, 1032 cm^{-1}), and symmetric M–F (M = Mo: 698; W: 716, 704 cm^{-1}) stretching modes of $[SF_3][M_2O_2F_9]$ are similar in frequency to previously reported $[SF_3]^+$[47] and $[M_2O_2F_9]^-$ salts. The vibrational modes of the anions were recently assigned in detail by Kraus and co-workers[25,27] as well as Schrobilgen and co-workers.[24] Upon solvation of $[SF_3][W_2O_2F_9]$ by HF, κ^1-O coordination to $[SF_3]^+$ by $[W_2O_2F_9]^-$ is evidenced by an increased splitting between the in-phase and out-of-phase ν(WO) modes (1030, 1013 cm^{-1}). Otherwise, the anion bands in the Raman spectra of solvated and unsolvated $[SF_3][W_2O_2F_9]$ are highly comparable. The absence of such pronounced splitting in unsolvated $[SF_3][W_2O_2F_9]$ would suggest that the anion does not coordinate through oxygen without solvation. The S–F stretching modes of the HF solvate (886–947 cm^{-1}) are red-shifted with respect to the unsolvated salt and more similar to those of $[SF_3][Mo_2O_2F_9]$, suggesting that HF is intermediate in its F-donor strength between $[Mo_2O_2F_9]^-$ and $[W_2O_2F_9]^-$ and insertion into an $S\cdots F_{eq}$ contact is only favoured in the tungsten-containing salt.

Fluorine-19 NMR Spectroscopy. The ^{19}F NMR spectrum of $MoOF_4(OSO)$ in SO_2 at –60 °C consists of a broad singlet at 154 ppm (Figure S4, $\Delta\nu_{1/2}$ = 610 Hz), consistent with SO_2 coordination *trans* to the oxido ligand.[35] The analogous sharp singlet for $WOF_4(OSO)$ (Figure S5, 74.9 ppm, $^1J_{WF}$ = 65.4 Hz) is highly comparable to that reported at ambient-temperature (73.9 ppm, $^1J_{WF}$ =

64 Hz).[48] The chemical shifts of the SO_2 adducts are higher in frequency than adducts with stronger donor ligands, such as CH_3CN (M = Mo: 146.5, W: 67.4 ppm) and $(C_6H_5)_3PO$ (M = Mo: 193.1, W: 60.5 ppm),[20,35] which is attributed to weaker electronic shielding by SO_2.

The broad cation (38 ppm, $\Delta\nu_{½}$ = 170 Hz) and anion (F_{eq}: 142 ppm, $\Delta\nu_{½}$ = 180 Hz; F_{ax}: –137 ppm, $\Delta\nu_{½}$ = 270 Hz) resonances of $[SF_3][Mo_2O_2F_9]$ in SO_2 at –60 °C (Figure S6) suggest exchange of the fluorido ligands between all three environments, considering that a resolved AX_8 spin system with ^{95}Mo satellites was observed for $[NO][Mo_2O_2F_9]$ in propylene carbonate at 10 °C.[29] Meanwhile, $[SF_3][W_2O_2F_9]$ gives rise to a sharp singlet (31.0 ppm) corresponding to the cation along with a resolved doublet (F_{eq}; 64.8 ppm, $^2J_{FF}$ = 57.8 Hz, $^1J_{WF}$ = 73.7 Hz) and nonet (F_{ax}; –146.4 ppm, $^1J_{WF}$ = 49.7 Hz) corresponding to the anion (Figure S7), as observed previously.[28] The chemical shift of the $[SF_3]^+$ resonance is at significantly higher frequency in the $[Mo_2O_2F_9]^-$ salt, indicating that its cation-anion interactions persist in solution, whereas in the $[W_2O_2F_9]^-$ analogue, the cation is solvated and the ions are discrete.

Computational Studies. The natural-population-analysis (NPA) charges, Wiberg valences, and Wiberg bond indices (WBIs) of MOF_4, $[WOF_4]_4$, $MOF_4(OSO)$, and $\{[SF_3][M_2O_2F_9]\}_2$ were calculated at the MN15/def2-SVPD level of theory and are given in Tables 5–7. As can be inferred from the NPA charges, the charge density on any given atom in monomeric MOF_4 is scarcely altered upon adduct formation with SO_2 (or, in the case of WOF_4, tetramerisation). Correspondingly, the WBIs predict little weakening of the M=O and M–F bonds, with those of $[WOF_4]_4$ even being slightly greater than those of WOF_4. Correspondingly, the WBIs of the contacts between WOF_4 subunits in $[WOF_4]_4$ (0.160), or between MOF_4 and SO_2 in $MOF_4(OSO)$ (M = Mo: 0.121, W: 0.128), indicate little covalent character in these interactions. Recent studies on the molecular electrostatic potential surfaces of MOF_4 reveal positive electrostatic potential (a

σ-hole) at the base of the square pyramid. As such, the weak contacts within $[WOF_4]_4$ and $MOF_4(OSO)$ are best interpreted as σ-hole bonding interactions that are largely electrostatic in nature.[24]

Fluoride-ion abstraction from SF_4 by MOF_4 to form $\{[SF_3][M_2O_2F_9]\}_2$ results in a polarisation of the MOF_4 moieties with respect to the parent MOF_4 molecules. The NPA charges on the terminal fluorido ligands in $\{[SF_3][M_2O_2F_9]\}_2$ (M = Mo: –0.458 to –0.471, W: –0.509 to –0.521) are of lesser magnitude than in MOF_4 (M = Mo: –0.472, W: –0.540). Conversely, those of the M–F···S bridging ligands are greater (M = Mo: –0.554 to –0.564, W: –0.589 to –0.602), though still lower than in the M–F–M bridging ligand (M = Mo: –0.659, W: –0.685). The WBIs of the M–F–M bridges (M = Mo: 0.235, 0.247; W: 0.231, 0.240) are approximately double those of the M···O contacts in $MOF_4(OSO)$, whereas those of the three strongest S···F contacts (M = Mo: 0.044–0.066, W: 0.045–0.061) are lesser and suggest predominantly electrostatic character in the cation-anion interactions. The fourth contact possesses negligible covalent character in both cases (WBI: 0.006).

Table 5. NPA Charges, Wiberg Valences,[a] and WBIs of MOF_4 and $[WOF_4]_4$[b]

	MOF_4		$[WOF_4]_4$
	M = Mo	**M = W**	
M(1)	+2.326 [4.978]	+2.784 [4.642]	+2.721 [4.722]
M(2)			+2.718 [4.725]
O(1)	–0.438 [2.341]	–0.626 [2.147]	–0.576 [2.206]
O(2)			–0.575 [2.207]
F(1)			–0.495 [0.931]
F(2)			–0.494 [0.932]
F(3)			–0.521 [0.891]
F(4)	–0.472 [0.963]	–0.540 [0.858]	–0.514 [0.902]
F(5)			–0.615 [0.769]
F(6)			–0.518 [0.894]
F(6)^{i}			–0.514 [0.902]
M(1)–O(1)	1.985	1.878	1.916
M(2)–O(2)			1.917
M(1)–F(1)			0.754
M(2)–F(2)			0.754
M(1)–F(3)			0.712
M(1)–F(4)	0.748	0.691	0.723
M(1)–F(5)			0.432
M(2)···F(5)			0.160
M(2)–F(6)			0.716
M(2)–F(6)^{i}			0.723

[a]Given in square brackets. [b]Calculated at the MN15/def2-SVPD level of theory. Symmetry transformation: i = 1 – x, y, 1 – z .

Table 6. NPA Charges, Wiberg Valences,[a] and WBIs of $MOF_4(OSO)$[b]

	M = Mo	M = W
M	+2.365 [4.962]	+2.700 [4.744]
O(1)	–0.459 [2.337]	–0.613 [2.170]
F(1)	–0.503 [0.921]	–0.548 [0.844]
F(2)	–0.490 [0.941]	–0.536 [0.863]
S	+1.672 [3.006]	+1.679 [3.001]
O(2)	–0.849 [1.843]	–0.863 [1.828]
O(3)	–0.742 [1.896]	–0.734 [1.903]
M–O(1)	1.969	1.874
M–F(1)	0.707	0.674
M–F(2)	0.724	0.691
M–O(2)	0.121	0.128
S–O(2)	1.384	1.367
S–O(3)	1.602	1.612

[a]Given in square brackets. [b]Calculated at the MN15/def2-SVPD level of theory.

Table 7. NPA Charges, Wiberg Valences,[a] and WBIs of $\{[SF_3][M_2O_2F_9]\}_2$[b]

	M = Mo	M = W		M = Mo	M = W
S	+2.136 [2.697]	+2.138 [2.696]	S–F(1)	0.824	0.828
F(1)	–0.420 [0.952]	–0.417 [0.956]	S–F(2)	0.829	0.834
F(2)	–0.418 [0.960]	–0.415 [0.965]	S–F(3)	0.832	0.833
F(3)	–0.416 [0.960]	–0.416 [0.961]	M(1)–O(1)	1.986	1.885
M(1)	+2.366 [4.971]	+2.707 [4.743]	M(2)–O(2)	1.990	1.885
M(2)	+2.371 [4.966]	+2.713 [4.736]	M(1)–F(4)	0.568	0.552
O(1)	–0.440 [2.353]	–0.599 [2.182]	M(1)–F(5)	0.772	0.734
O(2)	–0.438 [2.354]	–0.597 [2.183]	M(1)–F(6)	0.754	0.717
F(4)	–0.560 [0.827]	–0.592 [0.772]	M(1)–F(7)	0.634	0.601
F(5)	–0.458 [0.993]	–0.509 [0.909]	M(1)–F(8)	0.235	0.231
F(6)	–0.471 [0.973]	–0.521 [0.890]	M(2)–F(8)	0.247	0.240
F(7)	–0.552 [0.852]	–0.595 [0.777]	M(2)–F(9)	0.589	0.559
F(8)	–0.659 [0.831]	–0.685 [0.656]	M(2)–F(10)	0.770	0.733
F(9)	–0.564 [0.992]	–0.602 [0.766]	M(2)–F(11)	0.766	0.730
F(10)	–0.459 [0.992]	–0.510 [0.908]	M(2)–F(12)	0.583	0.563
F(11)	–0.463 [0.985]	–0.512 [0.903]	S···F(4)	0.066	0.061
F(12)	–0.554 [0.842]	–0.589 [0.782]	S···F(7)^{i}	0.006	0.006
			S···F(9)^{i}	0.044	0.045
			S···F(12)	0.061	0.057

[a]Given in square brackets. [b]Calculated at the MN15/def2-SVPD level of theory. Symmetry transformation: 1 – x, 1 – y, 1 – z

The WBIs of the S···F contacts do not readily suggest that HF insertion would be more likely for $\{[SF_3][W_2O_2F_9]\}_2$ than the molybdenum analogue. However, the NPA charges of the oxygen and fluorine atoms in the dimers indicate that in $\{[SF_3][W_2O_2F_9]\}_2$, the oxido ligands have higher charge density and are more basic than the terminal fluorido ligands, whereas in $\{[SF_3][Mo_2O_2F_9]\}_2$, the terminal fluorido ligands are the most basic sites. This could explain the occurrence of S···O chalcogen bonding in $[SF_3][W_2O_2F_9]\cdot HF$, though there is no evidence for such bonding in the Raman spectrum of unsolvated $[SF_3][W_2O_2F_9]$.

The calculated gas-phase thermochemical data for the monomerisation of $[WOF_4]_4$ by SO_2 predict a slightly endergonic reaction (13 kJ mol^{-1}), whereas by SF_4 it is predicted to be exergonic (−53 kJ mol^{-1}), reflective of the relative stabilities of $WOF_4(OSO)$ and $[SF_3][W_2O_2F_9]$ (Table 8).

Table 8. Gas-Phase Thermochemical Data for the Depolymerisation of $[WOF_4]_4$ by SO_2 and SF_4 at 25 °C[a]

Reaction	Δ_rG (kJ mol^{-1})	Δ_rH (kJ mol^{-1})	Δ_rS (J K^{-1})
$[WOF_4]_4 \rightarrow 4WOF_4$	88	240	510
$WOF_4 + SO_2 \rightarrow WOF_4(OSO)$	−19	−60	−139
$[WOF_4]_4 + 4SO_2 \rightarrow 4WOF_4(OSO)$	13	−1	−47
$[WOF_4]_4 + 2SF_4 \rightarrow \{[SF_3][W_2O_2F_9]\}_2$	−53	−148	−320

[a]Calculated at the MN15/def2-SVPD level of theory.

CONCLUSIONS

While the crystallographic reinvestigation of $[WOF_4]_4$ revealed that O/F disorder persists as low as −173 °C, optimising the structure of the tetramer in the gas phase revealed an asymmetric fluorine bridging motif unlike the symmetric bridging observed in $[MF_5]_4$ (M = Mo, W). The

reaction of MOF_4 with SO_2 and SF_4 resulted in the formation of $MOF_4(OSO)$ and $[SF_3][M_2O_2F_9]$, respectively, which were investigated crystallographically and spectroscopically. In particular, $[SF_3][W_2O_2F_9]$ was found to undergo HF insertion in aHF and aHF/SF_4 solvents, and the anion unusually forms chalcogen bonds through oxygen and fluorine to $[SF_3]^+$ in $[SF_3][W_2O_2F_9]\cdot HF$, rather than exclusively through fluorine as predicted for $\{[SF_3][W_2O_2F_9]\}_2$. Computational studies of $[WOF_4]_4$, $WOF_4(OSO)$, and $\{[SF_3][W_2O_2F_9]\}_2$ suggest that the W···F contacts of the tetramer are slightly stronger than the W···O contacts of the SO_2 adduct, rendering the latter thermodynamically unstable with respect to loss of SO_2 under ambient conditions. In contrast, formation of $[SF_3][W_2O_2F_9]$ is thermodynamically favourable.

EXPERIMENTAL

General Methods. All reactions were carried out in heat-sealed ¼"-o.d. FEP reactors that were connected to either 316-stainless-steel or Kel-F valves via flared fittings and passivated with F_2 (100%, Linde Gas). Sulfur dioxide was distilled on a Pyrex vacuum line equipped with high-vacuum PTFE valves. The transition-metal hexafluorides MoF_6 and WF_6, as well as SF_4 and aHF, were distilled through a nickel/316 stainless-steel vacuum line equipped with 316 stainless-steel valves (Autoclave Engineers) and pre-passivated with F_2. Solid materials were handled in a dry box (Omni Lab, Vacuum Atmospheres) under an atmosphere of dry N_2.

Sulfur dioxide (Matheson Gas) was dried over CaH_2. Sulfur tetrafluoride (Matheson Gas) was purified by distillation through activated charcoal. Anhydrous HF (Air Products, 99.9%) was dried with 100% F_2 and stored over $K_2[NiF_6]$. Molybdenum and tungsten hexafluoride (both Ozark-Mahoning) were used as provided. The oxide tetrafluorides $MoOF_4$[49] and WOF_4[50] were prepared as previously described.

Syntheses and Crystal Growth of $MOF_4(OSO)$. In the dry box, a flame-dried ¼"-o.d. glass reactor equipped with a grease-free PTFE valve (J. Young) was charged with $[WOF_4]_4$ (0.107 g, 0.388 mmol). Sulfur dioxide (*ca.* 0.2 mL) was then distilled into the reactor at –196 °C and the mixture was warmed to ambient temperature, resulting in a pale blue solution. The excess SO_2 was removed under dynamic vacuum at –70 °C for 1 h, affording $WOF_4(OSO)$ (0.137 g, 0.132 g expected for 100% yield w.r.t. $[WOF_4]_4$) as a white powder in quantitative yield. The $MoOF_4(OSO)$ adduct was prepared in an identical manner.

Colourless blocks of $MoOF_4(OSO)$ were grown by cooling an SO_2 solution (*ca.* 0.02 / 0.1 mL) in a ¼"-o.d. FEP reactor to –70 °C and storing at that temperature for 72 h, followed by removal of the excess SO_2 under dynamic vacuum at –70 °C for 15 min. Colourless blocks/plates of $WOF_4(OSO)$ were grown by cooling an SO_2 solution (*ca.* 0.02 g / 0.1 mL) in a ¼"-o.d. FEP reactor from –55 to –70 °C over 1 h, followed by removal of the excess SO_2 under dynamic vacuum at –70 °C for 15 min.

Syntheses and Crystal Growth of $[SF_3][M_2O_2F_9]$. In the dry box, a ¼"-o.d. FEP reactor was charged with $MoOF_4$ (0.045 g, 0.24 mmol). Sulfur tetrafluoride (*ca.* 0.1 mL) was then distilled into the reactor at –196 °C and the mixture was warmed towards ambient temperature until all solid dissolved, resulting in a colourless solution, before being cooled to –80 °C. The excess SF_4 was removed under dynamic vacuum at –80 °C for 1 h, affording $[SF_3][Mo_2O_2F_9]$ (0.058 g, 0.24 mmol) in quantitative yield. The $[SF_3][W_2O_2F_9]$ salt was prepared in an identical manner.

Colourless plates of $[SF_3][Mo_2O_2F_9]$ were grown in a ¼"-o.d. FEP reactor by removal of solvent from a solution in equal parts HF and SF_4 (*ca.* 0.02 g / 0.1 mL) under dynamic vacuum at –80 °C. Colourless blocks/plates of $[SF_3][W_2O_2F_9]\cdot HF$ were grown by rapidly cooling an aHF solution (*ca.* 0.02 g / 0.1 mL) in a ¼"-o.d. FEP reactor to –30 °C, after which the solution was

cooled to −75 °C over 2 h. The excess solvent was then removed under dynamic vacuum at that temperature for 2 h.

X-ray Crystallography. The reactors containing the crystals were cut on an aluminium trough that was positioned close to the diffractometer and cooled to *ca.* −80 °C by a stream of cold, dry N_2. Once the crystals were deposited onto the trough, the selected crystal was affixed to a Nylon cryo-loop submerged in perfluorinated polyether oil (Fomblin Z-25) and transferred to the goniometer using liquid-N_2-cooled cryo-tongs.

The crystals were centered on a Rigaku SuperNova diffractometer equipped with a Dectris Pilatus 3R 200K-A hybrid-pixel-array detector, a four-circle κ goniometer, an Oxford Cryostream 800 cooling device, and sealed MoKα and CuKα X-ray sources. Data were collected using the MoKα source (λ = 0.71073 Å) at −161 °C. Crystals were screened for quality before a pre-experiment was run to determine the unit cell, and a data-collection strategy was calculated based on the determined unit cell and intensity of the preliminary data. This strategy was optimized to collect five-fold redundant data at a resolution of 0.77 Å. The data were processed using CrysAlisPro,[51] which applied necessary Lorentz and polarization corrections to the integrated data and scaled the data. A numerical (Gaussian-grid) absorption correction was generated based upon the indexed faces of the crystal.

Atom positions were determined using the intrinsic phasing method (ShelXT)[52] and were refined using least-squares refinement (ShelXL).[53] Non-hydrogen atoms were refined anisotropically and recommended weights for the atoms were determined. In the case of $[SF_3][W_2O_2F_9]\cdot HF$, the position of the hydrogen atom was freely refined. The maximum and minimum electron density in the Fourier difference maps were located near the transition-metal

atom in all cases. Structure solution and refinement were performed with the aid of Olex2 (version 1.2).[54]

The crystallographic data were deposited with the CCDC/FIZ Karlsruhe joint service (CSD 2031683–2031687). Copies of the data can be obtained free of charge from CCDC via http://www.ccdc.cam.ac.uk.

Raman Spectroscopy. The Raman spectra were recorded using a Bruker RFS-100 Raman spectrometer outfitted with a quartz beam-splitter and liquid-N_2-cooled germanium detector. The 1064-nm line of a Nd:YAG laser was used for excitation of the sample, and backscattered (180°) radiation was sampled. The usable Stokes range of the collected data was 85−3500 cm^{-1} with a resolution of 2 cm^{-1}. The laser power was typically set to 50 mW for the molybdenum-containing samples, which fluoresced to some extent, and 150 mW for the tungsten-containing samples.

NMR Spectroscopy. The ^{19}F NMR spectra were recorded in heat-sealed 4-mm-o.d. FEP tubes sheathed in a 5-mm-o.d. glass insert using a Bruker Avance II 300 MHz spectrometer equipped with a 5-mm broadband probe. Spectra were recorded unlocked and referenced externally to $CFCl_3$ at 22 °C.

Computational Methods. The B3LYP, MN15, and PBE0 functionals, as implemented in Gaussian 16 (revision B.01),[55] along with the def2-SVPD basis set, obtained from the Basis Set Exchange,[56] were used for all atoms. The geometry of $MoOF_4(OSO)$ was optimised using all three functionals, which resulted in good agreement for the Mo=O and Mo–F bond lengths and angles, but excessive elongation of the Mo···O contact distance compared to the crystal structures when using B3LYP and PBE0 (> 0.14 Å, Table S5). As such, the MN15 functional was chosen for the remainder of the calculations as it reproduced the secondary bonding interactions most accurately (within 0.05 Å for $MoOF_4(OSO)$). Geometry optimisations were performed in the gas phase,

returning stationary points with all real frequencies except for C_{4h}-symmetric $[WOF_4]_4$ (*vide supra*). The NBO analyses were conducted using NBO (version 6.0).[57] GaussView (version 6.0) was used to visualise the vibrational modes and aid in their assignments.[58]

ASSOCIATED CONTENT

Supporting Information. The Supporting Information is available free of charge athttps://pubs.acs.org.

Crystallographic data collection and refinement parameters, experimental and calculated vibrational frequencies, Raman spectra of $[WOF_4]_4$ and $[SF_3][W_2O_2F_9]\cdot HF$, NMR spectra of $MOF_4(OSO)$ and $[SF_3][M_2O_2F_9]$, comparisons of calculated geometric parameters for $MOF_4(OSO)$ using the B3LYP, PBE0, and MN15 functionals.

ACKNOWLEDGEMENTS

We thank the Natural Sciences and Engineering Research Council of Canada for awarding Discovery grants to S.D.W., P. H., and M.G. as well as CGS-M and PGS-D scholarships to D.T. We thank Alberta Innovates - Technology Futures for awarding Graduate and Len Bolger Scholarships to P.C. The computational studies were performed using equipment funded through the Canada Foundation of Innovation as well as resources made available through Westgrid and Compute/Calcul Canada.

REFERENCES

(1) Young, N. A. Main Group Coordination Chemistry at Low Temperatures: A Review of Matrix Isolated Group 12 to Group 18 Complexes. *Coord. Chem. Rev.* **2013**, *257* (5–6), 956–1010. https://doi.org/10.1016/j.ccr.2012.10.013.

(2) Goettel, J. T.; Chaudhary, P.; Hazendonk, P.; Mercier, H. P. A.; Gerken, M. $SF_4 \cdot N(C_2H_5)_3$: The First Conclusively Characterized SF_4 Adduct with an Organic Base. *Chem. Commun.* **2012**, *48* (73), 9120. https://doi.org/10.1039/c2cc34578a.

(3) Chaudhary, P.; Goettel, J. T.; Mercier, H. P. A.; Sowlati-Hashjin, S.; Hazendonk, P.; Gerken, M. Lewis Acid Behavior of SF_4: Synthesis, Characterization, and Computational Study of Adducts of SF_4 with Pyridine and Pyridine Derivatives. *Chem. Eur. J.* **2015**, *21* (16), 6247–6256. https://doi.org/10.1002/chem.201406359.

(4) Kostiuk, N.; Goettel, J. T.; Gerken, M. Synthesis and Characterization of SF_4 Adducts with Polycyclic Amines. *Inorg. Chem.* **2020**. https://doi.org/10.1021/acs.inorgchem.0c01105.

(5) Smith, W. C. The Chemistry of Sulfur Tetraflouride. *Angew. Chem. Int. Ed. Engl.* **1962**, *1* (9), 467–475. https://doi.org/10.1002/anie.196204671.

(6) Kolditz, L. Halides of Arsenic and Antimony. In *Halogen Chemistry*; Gutmann, V., Ed.; Academic Press, 1967; p 115. https://doi.org/10.1016/b978-0-12-395589-0.x5001-9.

(7) Minkwitz, R.; Molsbeck, W.; Preut, H. Kristallstruktur von $SbF_5 \cdot SO_2$ / Crystal Structure of $SbF_5 \cdot SO_2$. *Z. Naturforsch. B* **1989**, *44* (12), 1581–1583. https://doi.org/10.1515/znb-1989-1218.

(8) Sajid, M.; Klose, A.; Birkmann, B.; Liang, L.; Schirmer, B.; Wiegand, T.; Eckert, H.; Lough, A. J.; Fröhlich, R.; Daniliuc, C. G.; Grimme, S.; Stephan, D. W.; Kehr, G.; Erker, G. Reactions of Phosphorus/Boron Frustrated Lewis Pairs with SO_2. *Chem. Sci.* **2013**, *4* (1), 213–219. https://doi.org/10.1039/c2sc21161k.

(9) Mingos, D. M. P. Sulphur Dioxide Complexes of the Platinum Metals. *Transit. Met. Chem.* **1978**, *3* (1), 1–15. https://doi.org/10.1007/BF01393495.

(10) Ryan, R. R.; Kubas, G. J.; Moody, D. C.; Eller, P. G. Structure and Bonding of Transition Metal-Sulfur Dioxide Complexes. In *Structure and Bonding 46 - Inorganic Chemistry*; Springer-Verlag Berlin Heidelberg GmbH: Berlin, Heidelberg, 1981; pp 47–100.

(11) Mews, R.; Lork, E.; Watson, P. G.; Görtler, B. Coordination Chemistry in and of Sulfur Dioxide. *Coord. Chem. Rev.* **2000**, *197* (1), 277–320. https://doi.org/10.1016/s0010-8545(99)00191-5.

(12) Jenne, C.; Lessen, V. Van. $Na^{+}[Me_3NB_{12}Cl_{11}]^{-}\cdot SO_2$: A Rare Example of a Sodium SO_2 Complex. *Acta Crystallogr. Sect. E Crystallogr. Commun.* **2019**, *75* (5), 607–610. https://doi.org/10.1107/S2056989019004663.

(13) Dirican, D.; Pfister, N.; Wozniak, M.; Braun, T. Reactivity of Binary and Ternary Sulfur Halides towards Transition-Metal Compounds. *Chem. Eur. J.* **2020**, *26* (31), 6945–6963. https://doi.org/10.1002/chem.201904493.

(14) Woolven, H.; González-Rodríguez, C.; Marco, I.; Thompson, A. L.; Willis, M. C. DABCO-Bis (Sulfur Dioxide), DABSO, as a Convenient Source of Sulfur Dioxide for Organic Synthesis: Utility in Sulfonamide and Sulfamide Preparation. *Org. Lett.* **2011**, *13* (18), 4876–4878. https://doi.org/10.1021/ol201957n.

(15) Turnbull, D.; Wetmore, S. D.; Gerken, M. Stabilization of $[WF_5]^{+}$ by Bidentate N-Donor Ligands. *Angew. Chem. Int. Ed.* **2019**, *58* (37), 13035–13038. https://doi.org/10.1002/anie.201906600.

(16) Grabowsky, S.; Luger, P.; Buschmann, J.; Schneider, T.; Schirmeister, T.; Sobolev, A. N.; Jayatilaka, D. The Significance of Ionic Bonding in Sulfur Dioxide: Bond Orders from X-Ray Diffraction Data. *Angew. Chem. Int. Ed.* **2012**, *51* (27), 6776–6779. https://doi.org/10.1002/anie.201200745.

(17) Edwards, A. J.; Jones, G. R. Fluoride Crystal Structures. Part I. Tungsten Oxide Tetrafluoride. *J. Chem. Soc. A* **1968**, 2074–2078. https://doi.org/10.1039/j19680002074.

(18) Bennett, M. J.; Haas, T. E.; Purdham, J. T. Structure and Bonding in the Tungsten Oxide Tetrafluoride Tetramer. *Inorg. Chem.* **1972**, *11* (1), 207–208. https://doi.org/10.1021/ic50107a053.

(19) Asprey, L. B.; Ryan, R. R.; Fukushima, E. Structure of Tungsten Oxytetrafluoride. *Inorg. Chem.* **1972**, *11* (12), 3122–3122. https://doi.org/10.1021/ic50118a053.

(20) Levason, W.; Reid, G.; Zhang, W. Coordination Complexes of the Tungsten(VI) Oxide Fluorides WOF_4 and WO_2F_2 with Neutral Oxygen- and Nitrogen-Donor Ligands. *J. Fluorine Chem.* **2016**, *184*, 50–57. https://doi.org/10.1016/j.jfluchem.2016.02.003.

(21) Emsley, J. W.; Levason, W.; Reid, G.; Zhang, W.; De Luca, G. Phosphine and Diphosphine Complexes of Tungsten(VI) Oxide Tetrafluoride. *J. Fluorine Chem.* **2017**, *197*, 74–79. https://doi.org/10.1016/j.jfluchem.2017.02.007.

(22) Mercier, H. P. A.; Breddemann, U.; Brock, D. S.; Bortolus, M. R.; Schrobilgen, G. J. Syntheses, Structures, and Bonding of $NgF_2 \cdot CrOF_4$, $NgF_2 \cdot 2CrOF_4$ (Ng = Kr, Xe), and $(CrOF_4)_\infty$. *Chem. Eur. J.* **2019**, *25* (52), 12105–12119. https://doi.org/10.1002/chem.201902005.

(23) Goettel, J. T.; Bortolus, M. R.; Stuart, D. G.; Mercier, H. P. A.; Schrobilgen, G. J. Chromium Oxide Tetrafluoride and Its Reactions with Xenon Hexafluoride; the $[XeF_5]^+$ and $[Xe_2F_{11}]^+$ Salts of the $[Cr^{VI}OF_5]^-$, $[Cr^{V}OF_5]^{2-}$, $[Cr^{V}_2O_2F_8]^{2-}$, and $[Cr^{IV}F_6]^{2-}$ Anions. *Chem. Eur. J.* **2019**, *25* (69), 15815–15829. https://doi.org/10.1002/chem.201903135.

(24) Bortolus, M. R.; Mercier, H. P. A.; Schrobilgen, G. J. Group 6 Oxyfluoro-Anion Salts of $[XeF_5]^+$ and $[Xe_2F_{11}]^+$: Syntheses and Structures of $[XeF_5][M_2O_2F_9]$ (M = Mo, W),

$[Xe_2F_{11}][M'OF_5]$ (M′ = Cr, Mo, W), $[XeF_5][HF_2]\cdot CrOF_4$, and $[XeF_5][WOF_5]\cdot XeOF_4$. *Chem. Eur. J.* **2020**, *26* (41), 8935–8950. https://doi.org/10.1002/chem.202000826.

(25) Stene, R. E.; Scheibe, B.; Karttunen, A. J.; Petry, W.; Kraus, F. Lewis Acidic Behavior of $MoOF_4$ towards the Alkali Metal Fluorides in Anhydrous Hydrogen Fluoride Solutions. *Eur. J. Inorg. Chem.* **2019**, *2019* (32), 3672–3682. https://doi.org/10.1002/ejic.201900595.

(26) Turnbull, D.; Gerken, M. Crystal Structure of an Ordered $[WOF_5]^-$ Salt: (1,10-Phen-H)$[WOF_5]$ (1,10-Phen = 1,10-Phenanthroline). *Acta. Crystallogr. E* **2020**, *76* (8), 1345–1348. https://doi.org/10.1107/S2056989020009767.

(27) Stene, R. E.; Scheibe, B.; Karttunen, A. J.; Petry, W.; Kraus, F. Synthesis and Characterization of $A[W_2O_2F_9]$ (A = Li–Cs). *Eur. J. Inorg. Chem.* **2020**, *2020* (23), 2260–2269. https://doi.org/10.1002/ejic.202000289.

(28) Rook, J. Some Studies of Transition Metal Chalcogenide Fluorides. PhD Thesis, University of Leicester: Leicester, England, **1987**.

(29) Bougon, R.; Bui Huy, T.; Charpin, P. Acid Properties of the Oxytetrafluorides of Molybdenum, Tungsten, and Uranium toward Some Inorganic Fluoride Ion Donors. *Inorg. Chem.* **1975**, *14* (8), 1822–1830. https://doi.org/10.1021/ic50150a016.

(30) Robiette, A. G.; Hedberg, K.; Hedberg, L. Gas-Phase Electron Diffraction Study of the Molecular Structure of Tungsten Oxytetrafluoride, WOF_4. *J. Mol. Struct.* **1977**, *37* (1), 105–112. https://doi.org/10.1016/0022-2860(77)87010-5.

(31) Edwards, A. J. Solid-State Structures of the Binary Fluorides of the Transition Metals. In *Advances in Inorganic Chemistry*; Academic Press, 1983; Vol. 27, pp 83–112. https://doi.org/10.1016/S0898-8838(08)60105-1.

(32) Stene, R. E.; Scheibe, B.; Pietzonka, C.; Karttunen, A. J.; Petry, W.; Kraus, F. MoF_5 Revisited. A Comprehensive Study of MoF_5. *J. Fluorine Chem.* **2018**, *211*, 171–179. https://doi.org/10.1016/J.JFLUCHEM.2018.05.002.

(33) Stene, R.; Scheibe, B.; Ivlev, S. I.; Karttunen, A. J.; Petry, W.; Kraus, F. Photochemical Synthesis of Tungsten Pentafluoride, WF 5. *Z. Anorg. Allg. Chem.* **2020**. https://doi.org/10.1002/zaac.202000177.

(34) Turnbull, D.; Wetmore, S. D.; Gerken, M. Synthesis, Characterization, and Lewis-Acid Behaviour of $[W(NC_6F_5)F_4]_x$, and Computational Study of $W(NR)F_4$ (R = H, F, CH_3, CF_3, C_6H_5, C_6F_5), $W(NC_6F_5)F_4(NCCH_3)$, and $W(NC_6F_5)F_4(NC_5H_5)_n$ (n = 1, 2). *Inorg. Chem.* **2019**, *58* (9), 6363–6375. https://doi.org/10.1021/acs.inorgchem.9b00574.

(35) Levason, W.; Monzittu, F. M.; Reid, G.; Zhang, W.; Hope, E. G. Complexes of Molybdenum(VI) Oxide Tetrafluoride and Molybdenum(VI) Dioxide Difluoride with Neutral N- and O-Donor Ligands. *J. Fluorine Chem.* **2017**, *200*, 190–197. https://doi.org/10.1016/j.jfluchem.2017.06.015.

(36) Gibler, D. D.; Adams, C. J.; Fischer, M.; Zålkin, A.; Bartlett, N. Structural Studies of Trifluorosulfur(IV)yl, $[SF_3]^+$, Salts Including the Crystal Structure of $[SF_3]^+[BF_4]^-$. *Inorg. Chem.* **1972**, *11* (10), 2325–2329. https://doi.org/10.1021/ic50116a007.

(37) Mallouk, T. E.; Rosenthal, G. L.; Müller, G.; Brusasco, R.; Bartlett, N. Fluoride Ion Affinities of GeF_4 and BF_3 from Thermodynamic and Structural Data for $(SF_3)_2GeF_6$, ClO_2GeF_5, and ClO_2BF_4. *Inorg. Chem.* **1984**, *23* (20), 3167–3173. https://doi.org/10.1021/ic00188a028.

(38) Smith, G. L.; Schrobilgen, G. J. On the Reactivity of $F_3S{\equiv}NXeF^+$: Syntheses and Structural Characterizations of $[F_4S{=}N{-}Xe{-}N{\equiv}SF_3][AsF_6]$, a Rare Example of a N–Xe–N Linkage, and

$[F_3S(N{\equiv}SF_3)_2][AsF_6]$. *Inorg. Chem.* **2009**, *48* (16), 7714–7728. https://doi.org/10.1021/ic900651n.

(39) Goettel, J. T.; Gerken, M. Synthesis and Characterization of Adducts between SF_4 and Oxygen Bases: Examples of O···S(IV) Chalcogen Bonding. *Inorg. Chem.* **2016**, *55* (23), 12441–12450. https://doi.org/10.1021/acs.inorgchem.6b02373.

(40) Alvarez, S. A Cartography of the van Der Waals Territories. *Dalton Trans.* **2013**, *42* (24), 8617–8636. https://doi.org/10.1039/c3dt50599e.

(41) Küster, R.; Drews, T.; Seppelt, K. The Trifluorophosphonium Ion, PF_3H^+, Preparation and Structure. *Inorg. Chem.* **2000**, *39* (13), 2784–2786. https://doi.org/10.1021/ic991420w.

(42) Hoskins, B. F.; Linden, A.; O'Donnell, T. A. Controlled Hydrolysis of the Hexafluorides of Molybdenum, Tungsten and Rhenium: Structure of Oxonium (μ-Fluoro)Bis(Tetrafluorooxotungstate(VI)). *Inorg. Chem.* **1987**, *26* (14), 2223–2228. https://doi.org/10.1021/ic00261a012.

(43) Arnaudet, L.; Bougon, R.; Ban, B.; Lance, M.; Navaza, A.; Nierlich, M.; Vigner, J. Structure of the New Fluoro Complex of Tungsten(VI): $[WF_4(bipy)_2]_2^{+}{\cdot}2[W_2O_2F_9]^{-}{\cdot}0.25HF$ (bipy = 2,2′-bipyridyl). *J. Fluorine Chem.* **1992**, *59* (1), 141–152. https://doi.org/10.1016/S0022-1139(00)80212-2.

(44) Crossman, M. C.; Fawcett, J.; Hope, E. G.; Russell, D. R. Crystal Structure of μ^2-Hydridododecacarbonyltriosmium Dioxooctafluoro-μ^2-Fluoroditungsten. *J. Organomet. Chem.* **1996**, *514* (1–2), 87–91. https://doi.org/10.1016/0022-328X(95)06012-L.

(45) Beattie, I. R.; Livingston, K. M. S.; Reynolds, D. J.; Ozin, G. A. Vibrational Spectra of Some Oxide Halides of the Transition Elements with Particular Reference to Gas-Phase and

Single-Crystal Raman Spectroscopy. *J. Chem. Soc. A* **1970**, No. 0, 1210–1216. https://doi.org/10.1039/J19700001210.

(46) Anderson, A.; Campbell, M. C. W. Infrared and Raman Spectra of Crystalline Sulfur Dioxide. *J. Chem. Phys.* **1977**, *67* (9), 4300–4302. https://doi.org/10.1063/1.435371.

(47) Azeem, M.; Brownstein, M.; Gillespie, R. J. An Investigation of the Structures of the Adducts of SF_4 with BF_3, PF_5, AsF_5, and SbF_5 in the Solid State and in Solution in HF. *Can. J. Chem.* **1969**, *47* (22), 4159–4167. https://doi.org/10.1139/v69-689.

(48) Tebbe, F. N.; Muetterties, E. L. Further Evidence of Stereochemical Nonrigidity in Five- and Seven-Coordinate Structures. *Inorg. Chem.* **1968**, *7* (1), 172–174.

(49) Bougon, R.; Bui Huy, T.; Charpin, P. Acid Properties of the Oxytetrafluorides of Molybdenum, Tungsten, and Uranium toward Some Inorganic Fluoride Ion Donors. *Inorg. Chem.* **1975**, *14* (8), 1822–1830. https://doi.org/10.1021/ic50150a016.

(50) Selig, H.; Sunder, W. A.; Schilling, F. C.; Falconer, W. E. Hydrolysis Reactions of Transition Metal Fluorides in Liquid Hydrogen Fluoride: Oxonium Salts with Nb, Ta and W. *J. Fluorine Chem.* **1978**, *11* (6), 629–635. https://doi.org/10.1016/S0022-1139(00)81621-8.

(51) Wilson, W. W.; Christe, K. O.; Bougon, R. Tungsten Tetrafluoride Oxide. In *Inorganic Syntheses, Volume 24*; Wiley, 1986; pp 37–38. https://doi.org/10.1002/9780470132555.ch12.

(52) CrysAlisPro, version 171.38.43. Agilent Technologies, Ltd.: Yarnton, Oxfordshire, England, **2014**.

(53) Sheldrick, G. M. SHELXT – Integrated Space-Group and Crystal-Structure Determination. *Acta Crystallogr. A* **2015**, *71* (1), 3–8. https://doi.org/10.1107/S2053273314026370.

(54) Sheldrick, G. M. Crystal Structure Refinement with SHELXL. *Acta Crystallogr. C* **2015**, *71* (1), 3–8. https://doi.org/10.1107/S2053229614024218.

(55) Dolomanov, O. V.; Bourhis, L. J.; Gildea, R. J.; Howard, J. A. K.; Puschmann, H. OLEX2 : A Complete Structure Solution, Refinement and Analysis Program. *J. Appl. Crystallogr.* **2009**, *42* (2), 339–341. https://doi.org/10.1107/S0021889808042726.

(56) Gaussian 16, revision B.01. Frisch, M. J.; Trucks, G. W.; Schlegel, H. B.; Scuseria, G. E.; Robb, M. A.; Cheeseman, J. R.; Scalmani, G.; Barone, V.; Petersson, G. A.; Nakatsuji, H.; Li, X.; Caricato, M.; Marenich, A. V.; Bloino, J.; Janesko, B. G.; Gomperts, R.; Mennucci, B.; Hratchian, H. P.; Ortiz, J. V.; Izmaylov, A. F.; Sonnenberg, J. L.; Williams-Young, D.; Ding, F.; Lipparini, F.; Egidi, F.; Goings, J.; Peng, B.; Petrone, A.; Henderson, T.; Ranasinghe, D.; Zakrzewski, V. G.; Gao, J.; Rega, N.; Zheng, G.; Liang, W.; Hada, M.; Ehara, M.; Toyota, K.; Fukuda, R.; Hasegawa, J.; Ishida, M.; Nakajima, T.; Honda, Y.; Kitao, O.; Nakai, H.; Vreven, T.; Throssell, K.; Montgomery, J. A., Jr.; Peralta, J. E.; Ogliaro, F.; Bearpark, M. J.; Heyd, J. J.; Brothers, E. N.; Kudin, K. N.; Staroverov, V. N.; Keith, T. A.; Kobayashi, R.; Normand, J.; Raghavachari, K.; Rendell, A. P.; Burant, J. C.; Iyengar, S. S.; Tomasi, J.; Cossi, M.; Millam, J. M.; Klene, M.; Adamo, C.; Cammi, R.; Ochterski, J. W.; Martin, R. L.; Morokuma, K.; Farkas, O.; Foresman, J. B.; Fox, D. J. Gaussian, Inc.: Wallingford, CT, USA, **2016**.

(57) Pritchard, B. P.; Altarawy, D.; Didier, B.; Gibson, T. D.; Windus, T. L. New Basis Set Exchange: An Open, Up-to-Date Resource for the Molecular Sciences Community. *J. Chem. Inf. Model.* **2019**, *59* (11), 4814–4820. https://doi.org/10.1021/acs.jcim.9b00725.

(58) NBO, version 6.0. Glendening, E. D.; Badenhoop, J. K.; Reed, A. E.; Carpenter, J. E.; Bohmann, J. A.; Morales, C. M.; Landis, C. R.; Weinhold, F. NBO. Theoretical Chemistry Institute, University of Wisconsin: Madison, WI, USA, **2013**.

(59) GaussView, version 6.0. Dennington, R.; Keith, T. A.; Millam, J. M. GaussView. Semichem, Inc.: Shawnee Mission, KS, USA, **2016**.

Table of Contents Synopsis and Graphic

Molybdenum and tungsten oxide tetrafluoride, MOF_4 (M = Mo, W), were reacted with SO_2 and SF_4, yielding $MOF_4(OSO)$ and $[SF_3][M_2O_2F_9]$, respectively. The crystal structures of $MOF_4(OSO)$ reveal that SO_2 undergoes κ^1-O coordination to MOF_4 *trans* to the oxido ligand. In the crystal structure of $[SF_3][Mo_2O_2F_9]$, $[SF_3]^+$ is chelated (κ^2-F) by $[Mo_2O_2F_9]^-$ and these ion pairs dimerise, resulting in heptacoordinate sulfur centres. Meanwhile, in $[SF_3][W_2O_2F_9]\cdot HF$, $[W_2O_2F_9]^-$ hydrogen bonds with HF and unusually coordinates through fluorine and oxygen to separate $[SF_3]^+$ cations.

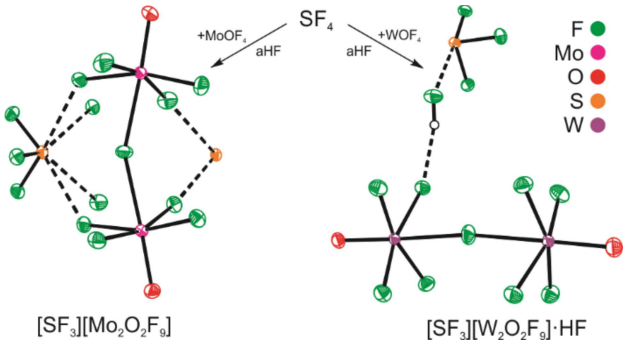

For Table of Contents only.